



1 **Changes in productivity and intermediate circulation in the**
2 **northern Indian Ocean since the last deglaciation: new**
3 **insights from benthic foraminiferal Cd/Ca records and**
4 **benthic assemblage analyses**

5 Ruifang Ma^{1,2*}, Sophie S épulcre¹, Laetitia Licari³, Frédéric Haurine¹, Franck Bassinot⁴,
6 Zhaojie Yu⁵, Christophe Colin¹

7 ¹ GEOPS, Université Paris-Saclay, CNRS, Orsay, 91405, France.

8 ² State Key Laboratory of Cryospheric Science, Northwest Institute of Eco-Environment and Resources, Chinese
9 Academy of Sciences, Lanzhou, 730000, China.

10 ³ CEREGE, Aix-Marseille Université-Europole de l'Arbois-BP80, Aix-en-Provence, 13545, France.

11 ⁴ LSCE/IPSL, CEA CNRS UVSQ, Gif Sur Yvette, F-91190, France.

12 ⁵ Key Laboratory of Marine Geology and Environment, Institute of Oceanology, Chinese Academy of Sciences,
13 Qingdao, 266071, China.

15 *Correspondence to: R. MA (maruifang89@hotmail.com)

16
17 **Abstract.** We have measured Cd/Ca ratios of several benthic foraminiferal species and studied benthic
18 foraminiferal assemblages on two cores from the northern Indian Ocean (Arabian Sea and northern Bay of
19 Bengal, BoB), in order to reconstruct variations in intermediate water circulation and paleo-nutrient content
20 since the last deglaciation. Intermediate water Cd_w records estimated from the benthic Cd/Ca reflect past changes
21 in surface productivity and/or intermediate-bottom water ventilation. The benthic foraminiferal assemblages are
22 consistent with the geochemical data. These results suggest that during the last deglaciation, the Heinrich Stadial
23 1 and Younger Dryas (HS1 and YD, respectively) millennial-scale events were marked by a decrease in Cd_w
24 values, indicating an enhanced ventilation of intermediate-bottom water masses. Benthic foraminifer
25 assemblages indicate that surface primary productivity was low during the early Holocene (from 10 to 6 cal kyr
26 BP), resulting in low intermediate water Cd_w at both sites. From ~5.2 to 2.4 cal kyr BP, the benthic
27 foraminiferal assemblages indicate meso- to eutrophic intermediate water conditions, which correspond to high
28 surface productivity. This is consistent with a significant increase in the intermediate water Cd_w in the
29 southeastern Arabian Sea and the northeastern BoB. The comparison of intermediate water Cd_w records with
30 previous reconstructions of past Indian monsoon evolution during the Holocene suggests a direct control of
31 intermediate water Cd_w by monsoon-induced changes in upper water stratification and surface primary
32 productivity.

33
34 **1. Introduction**

35 During the last deglaciation, a two-step rapid increase in atmospheric CO₂ occurred during the 18-14.7 and
36 12.8-11.7 cal kyr BP time intervals (e.g., Monnin et al., 2001). Several studies suggest that variations in the
37 Southern Ocean circulation contributed to these increases in atmospheric CO₂ by transferring deep ocean carbon
38 to the upper ocean and atmosphere, through enhanced upwelling and increased northward penetration of the
39 Antarctic Intermediate Water (AAIW) in all ocean basins (e.g., Marchitto et al., 2007; Anderson et al., 2009;
40 Skinner et al., 2014). Different proxies have been used to reconstruct past changes in intermediate circulation,



41 such as radiocarbon activity ($\Delta^{14}\text{C}$) (e.g., Marchitto et al., 2007; Bryan et al., 2010), benthic $\delta^{13}\text{C}$ (e.g., Pahnke
42 and Zahn, 2005; Jung et al., 2009; Ma et al., 2019), foraminiferal ε_{Nd} (e.g., Pahnke et al., 2008; Xie et al., 2012;
43 Yu et al., 2018) and benthic foraminifera Sr/Ca (Ma et al., 2020). These studies have focused on the close
44 relationship between enhanced ventilation in the Southern Ocean and rising atmospheric CO_2 during the last
45 deglaciation period. Furthermore, it has been shown that glacial-interglacial transfer of CO_2 between the oceans
46 and the atmosphere could also be linked to changes in the efficiency of the oceanic biological pump (Pichevin et
47 al., 2009; Ziegler et al., 2013; Bauska et al., 2016; Hertzberg et al., 2016; Jaccard et al., 2016; Yu et al., 2019),
48 which may contribute up to half of the observed CO_2 flux (Kohfeld, 2005).

49 The oceanic biological pump and nutrient upwelling are at least partly controlled by intermediate-deep water
50 circulation, contributing to the observed CO_2 changes (e.g., Toggweiler, 1999; Marchitto and Broecker, 2006).
51 To track past changes in the nutrient concentration of intermediate water masses, benthic foraminifera Cd/Ca has
52 been used in many recent studies (e.g. Came et al., 2008; Poggemann et al., 2017; Valley et al., 2017; Umling et
53 al., 2018); indeed, the benthic foraminifera Cd/Ca is a robust proxy of seawater cadmium concentrations (Cd_w)
54 (Boyle, 1988; 1992), which shows a positive linear correlation with labile nutrients (phosphate and nitrate) in the
55 modern ocean (e.g., Boyle et al., 1976; Boyle, 1988; Elderfield and Rickaby, 2000). The benthic foraminifera
56 incorporate Cd as a function of Cd_w with a species-dependent partition coefficient (e.g., Tachikawa and
57 Elderfield, 2002). Thus, the Cd measured in the fossil tests reflects the paleo-nutrient concentrations of the
58 surrounding water masses, and can be used to investigate past changes in intermediate-to-deep ocean properties
59 (e.g., Boyle and Keigwin, 1982; Oppo and Fairbanks, 1987; Came et al., 2008; Poggemann et al., 2017; Valley et
60 al., 2017; Umling et al., 2018).

61 Complementary to the geochemical proxies, the type of benthic foraminifers and their abundance, both of
62 which are related to organic flux and ecosystem oxygenation, make benthic foraminifer assemblages a powerful
63 proxy for estimating past variations in bottom water conditions (e.g., Corliss et al., 1986; Schmiiedl et al., 1998;
64 Almogi-Labin et al., 2000) in conjunction with organic matter fluxes to the seafloor (e.g., Altenbach et al., 1999;
65 Van der Zwaan et al., 1999; Fontanier et al., 2002; Caille et al., 2015). Benthic foraminifera have been
66 successfully used as indicators of surface productivity, especially in high carbon flux regions (Schnitker, 1994).
67 By comparing past benthic foraminiferal assemblages to modern ones, changes in food supply and oxygen
68 concentrations of the bottom water can be reconstructed (e.g., Corliss, 1979; Peterson, 1984; Murgese and De
69 Deckker, 2005). Recently, the combining of benthic foraminiferal assemblages and geochemical proxies has
70 received increasing attention and have been used to reconstruct the evolution of surface productivity and
71 upwelling intensity in the Indian Ocean (e.g., Hermelin 1991, 1992; Hermelin and Shimmield, 1995; Den Dulk
72 et al., 1998; Murgese and De Deckker, 2005).

73 The Arabian Sea is one of the most productive regions of the ocean today (Banse, 1987; Marra and Barber,
74 2005). Surface productivity is dominated by the monsoon system, which has a strong impact on the distribution
75 and dynamics of stratification and vertical mixing (L' y et al., 2007). Numerous studies have focused on the
76 reconstruction of the paleo-productivity of the Arabian Sea in relation to past changes in monsoon intensity (e.g.,
77 Prell and Kutzbach, 1987; Naidu and Malmgren, 1996; Gupta et al., 2003; Singh et al., 2006; 2011; Bassinot et
78 al., 2011; Saraswat et al., 2014). By contrast, little is known about the paleoproductivity of the BoB (Phillips et
79 al., 2014; Zhou et al., 2020). Furthermore, the evolution of the nutrient content of intermediate water masses
80 since the last deglaciation has never been reconstructed in the Indian Ocean, where only two low-resolution



81 Cd/Ca records are available for deep-water depths (Boyle et al., 1995), and, to our knowledge, none are available
82 for intermediate water depths.

83 In this study, we provide, for the first time, two benthic foraminifera Cd/Ca records at intermediate water
84 depths in the northern Indian Ocean (Arabian Sea and northern Bay of Bengal). These data make it possible to
85 estimate past changes in the nutrient content, since the last deglaciation, over the last 17 kyr BP. We have also
86 investigated benthic foraminiferal assemblages obtained from core MD77-191 (southeastern Arabian Sea) to
87 help us reconstruct the conditions at the seafloor. Combined with planktonic foraminiferal $\delta^{18}\text{O}$, benthic $\delta^{13}\text{C}$,
88 and Cd/Ca records obtained from the same core, as well as with results already published in the Bay of Bengal
89 (Ma et al., 2019; 2020), this study aims to document past variations in intermediate- and deep-water conditions
90 and to decipher their links with surface paleo-productivity and intermediate water ventilation.

91

92 **2. Material and modern hydrological setting**

93

94 We analyzed sediment core MD77-191 (07°30'N-76°43'E, 1254m) located in the Arabian Sea (off the
95 southern tip of India), and core MD77-176 (14°30'5N-93°07'6E, 1375m) retrieved in the northeastern Bay of
96 Bengal (BoB). These cores were collected in 1977 during the OSIRIS III cruise of the French N/O Marion
97 Dufresne (Fig. 1).

98 The age model of core MD77-191 was established by using accelerator mass spectrometry (AMS) ^{14}C dates
99 obtained on 9 monospecific samples of planktonic foraminifera *Globigerinoides bulloides* (Bassinot et al., 2011),
100 one sample of pteropods (Ml éneck, 1997), and three samples of planktonic foraminifera *Globigerinoides ruber*
101 (Ma et al., 2020). The average sedimentation rate of core MD77-191 is about 53 cm.kyr⁻¹ and up to 90 cm.kyr⁻¹
102 during the Holocene, providing a high-resolution, continuous record since 17 cal kyr BP.

103 The age model of core MD77-176 was previously established by using 31 planktonic foraminifer (*G. ruber*)
104 AMS ^{14}C dates combined with the core MD77-176 oxygen isotope record obtained on planktonic foraminifera *G.*
105 *ruber*, which were correlated to the GISP2 Greenland ice core record (Marzin et al., 2013). Core MD77-176
106 displays high accumulation rates (average ~25 cm.kyr⁻¹ and up to 40 cm.kyr⁻¹ during the Holocene).

107 In the modern ocean, the surface waters of the Arabian Sea and BoB are characterized by seasonally reversing
108 currents that are driven by the monsoon winds (Fig1.a). The surface water masses shallower than 150 m in the
109 Arabian Sea are mainly Arabian Sea high Salinity Water (ASHS, 36.5 psu) (Talley et al., 2011). In the BoB, the
110 surface waters above 100 m are designated Bay of Bengal surface waters (BoBSW), which have a low salinity
111 (31 psu) due to large river inputs (Talley et al., 2011). Today, the northward extension of AAIW in the Indian
112 Ocean rarely reaches beyond 10°S (Lynch-Stieglitz et al., 1994). The sites of cores MD77-191 and MD77-176
113 are mainly bathed, therefore, by the North Indian Intermediate Water (Olson et al., 1993; Reid, 2003) with a
114 potential contribution from the Red Sea Outflow Water (RSOW) for the site MD77-191 (Beal et al., 2000) and
115 from the southern return flow of deep water (North Indian Deep Water) for the site of core MD77-176 (Talley et
116 al., 2011).

117 As far as surface waters are concerned, during the summer monsoon, the clockwise circulation in the
118 Arabian Sea drives high salinity waters from the northern to the southeastern Arabian Sea (Fig. 1 and S1). By
119 contrast, during the winter monsoon, the northeastern winds bring low salinity water (BoBSW) from the BoB.
120 The northern Indian Ocean, especially the Arabian Sea, is characterized by highly variable seasonal productivity



121 (Shankar et al., 2002). Southwest winds during the summer season induce a strong Ekman pumping resulting in
122 very active upwelling along the western coasts of the Arabian Sea and thus promoting strong surface
123 productivity (Shankar et al., 2002; Fig. S1). By contrast, the surface productivity in the BoB is generally weak
124 compared with the Arabian Sea (e.g., Prasanna Kumar et al., 2001; Thushara and Vinayachandran, 2016;
125 O'Malley, 2017; Fig. S1). In the BoB, large river inputs of fresh water and direct monsoon precipitation lead to
126 more stable stratification in the upper ocean (Vinayachandran et al., 2002), and hence the vertical mixing of
127 nutrients from the subsurface to the euphotic zone is generally limited (Gomes et al., 2000). However, the
128 primary productivity of the western BoB shows a slight increase during the winter monsoon, as indicated by the
129 distribution of chlorophyll in the surface water (Thushara and Vinayachandran, 2016; O'Malley, 2017; Fig. S1).

130 Modern data indicate that the southern-sourced intermediate water (AAIW) in the Indian Ocean has a
131 phosphate concentration of about 2-2.5 $\mu\text{mol/kg}$ (Figs. 1b and c). In the Northern intermediate Indian Ocean, the
132 phosphate concentration is significantly higher, ranging from 2.75 to 3 $\mu\text{mol/kg}$ in the Arabian Sea during the
133 summer monsoon, and from 2.5 to 2.75 $\mu\text{mol/kg}$ in the BoB during the winter monsoon (Figs. 1b and c). The
134 higher phosphate in the northern Indian Ocean can be linked to primary productivity (Banse, 1987; Marra and
135 Barber, 2005).

136

137 3. Methods

138 3.1. Cd/Ca analysis

139

140 We analyzed Cd/Ca in three calcite (*Cibicidoides pachyderma*, *Uvigerina peregrina*, and *Globobulimina* spp.)
141 and one aragonite (*Hoeglundina elegans*) benthic foraminiferal species from core MD77-191. *C. pachyderma* is
142 an epifaunal species, *U. peregrina* and *Globobulimina* spp. are endobenthic species with intermediate and deep
143 microhabitats, respectively (Fontanier et al., 2002). In core MD77-176, due to the limitation of calcitic species,
144 we only measured Cd/Ca ratios in *H. elegans* shells.

145 Each sample contained between 10 and 15 individuals picked from the 250-315 μm size fraction. Samples
146 were gently crushed, cleaned to remove clays, organic matter and elemental oxides by using reductive and
147 oxidative cleaning following previously published methods (Boyle and Keigwin, 1982; Barker et al., 2003).
148 Each sample was dissolved in 0.075N HNO_3 and analyzed using a single collector sector field high resolution
149 inductively coupled plasma mass spectrometer (HR-ICP-MS) Thermo Element XR hosted at the GEOPS
150 Laboratory (University Paris-Saclay, France).

151 The detailed instrumental settings and mother standard solutions are described in Ma et al., (2020). A blank
152 consisting of the same 0.1N HNO_3 used to dilute the standards and samples was also analyzed. We removed the
153 blank intensity values from all the raw intensities (including standards), and raw data were linearly drift-
154 corrected by interspersing a drift standard every four samples. Standard curves were used to calculate elemental
155 concentrations, coefficients of determination (r^2) always being >0.9999 for all elemental ratios. The mean
156 reproducibility and accuracy are 3.6% and 7.5%, respectively.

157

158 3.2 Faunal analysis

159

160 Benthic foraminiferal assemblages from core MD77-176 have already been published in Ma et al. (2019). For
161 core MD77-191, a total of 72 samples were collected for benthic foraminiferal assemblage determinations. In
162 each sample, benthic foraminifera ($>150 \mu\text{m}$) were extracted, counted and identified to species level following



163 the taxonomical descriptions of various authors (e.g., Loeblich and Tappan, 1988; Jones, 1994; Holbourn et al.,
164 2013). For core MD77-191, there is no material left in this old, low diameter core and so we used samples
165 obtained earlier for stable isotope studies. Since the bulk weights of these samples were not recorded prior to
166 sieving, we could not perform the calculation of absolute abundance of foraminifera or accumulation rates. Thus,
167 we only converted the individual counts to percentages with respect to the total benthic foraminifera present in
168 each sample. In order to describe major faunal variations, we performed principal component analysis (PCA)
169 using the PAST software (Version 3.0, Hammer et al., 2001). Species present with a percentage >1% in at least 1
170 sample were used for statistical analysis and diversity calculation.

171

172 **4. Results**

173

174 **4.1. Elemental ratios results**

175

176 To check the influence of oxide contaminants on the elemental ratios, Mn/Ca was systematically measured.
177 The Mn/Ca of *H. elegans* from cores MD77-191 and MD77-176 ranges between 6.5-10 $\mu\text{mol/mol}$ and 1-30
178 $\mu\text{mol/mol}$, respectively. Such ranges are much lower than the 100 $\mu\text{mol/mol}$ limit proposed by Boyle (1983).
179 The Mn/Ca obtained on the three calcite benthic foraminifera species from core MD77-191 - *C. pachyderma* (5-
180 18 $\mu\text{mol/mol}$), *U. peregrina* (3-23 $\mu\text{mol/mol}$) and *Globobulimina* spp. (4-69 $\mu\text{mol/mol}$) - are also all below 100
181 $\mu\text{mol/mol}$ (Boyle, 1983). The Fe/Ca ratios are also lower than 1 mmol/mol in all samples from cores MD77-191
182 and MD77-176, in agreement with the limit proposed by Barker et al. (2003). In addition, Barker et al. (2003)
183 concluded that no significant pollution by clay minerals would be expected when Al/Ca is <0.5 mmol/mol . In all
184 our samples, Al/Ca is below 0.5 mmol/mol , indicating that the sample cleaning procedure was efficient.

185 All of the above results indicate that our samples were not affected by contamination.

186

187 **4.1.1 Cd/Ca**

188

189 The Cd/Ca records of *C. pachyderma*, *U. peregrina* and *Globobulimina* spp. from core MD77-191 range
190 between 0.07-0.2 $\mu\text{mol/mol}$, 0.07-0.14 $\mu\text{mol/mol}$ and 0.03-0.09 $\mu\text{mol/mol}$, respectively (Figs. 2e-g;
191 supplementary Table S1).

192 The Cd/Ca records for the calcite benthic species *C. pachyderma* and *U. peregrina* have very low time
193 resolutions during the last deglaciation. However, some common patterns can be observed. The Cd/Ca records of
194 *C. pachyderma* and *U. peregrina* show lower values during the Heinrich stadial 1 (HS1, 17-15.2 cal kyr BP) and
195 Younger Dryas (YD, 12-11 cal kyr BP) cold periods, with average values of ~ 0.08 $\mu\text{mol/mol}$ for *C. pachyderma*
196 and ~ 0.09 $\mu\text{mol/mol}$ for *U. peregrina*. By contrast, these two species display higher Cd/Ca ratios (~ 0.12
197 $\mu\text{mol/mol}$) during the Bølling-Allerød warm period (B-A, 15-13.3 cal kyr BP) compared with the HS1 and YD.
198 Then, lower values (~ 0.1 $\mu\text{mol/mol}$ for *C. pachyderma*; 0.11 $\mu\text{mol/mol}$ for *U. peregrina*) are observed during the
199 early Holocene (10-5 cal kyr BP) compared to larger variations occurring in the late Holocene (5.2-2.4 cal kyr
200 BP). The Cd/Ca record of deep infaunal *Globobulimina* spp., obtained at a lower time resolution, shows different
201 variations compared with the two other taxa without any clear trend during the Holocene.

202 The *H. elegans* Cd/Ca values of core MD77-191 range from 0.05 to 0.31 $\mu\text{mol/mol}$ since 17 cal kyr BP (Fig.
203 2d; supplementary Table S1). Depleted values at about 0.07 $\mu\text{mol/mol}$ are recorded from the last deglaciation to
204 the early Holocene (17-5 cal kyr BP time interval). During the HS1 and the YD time intervals over the last
205 deglaciation, significant decrease of about ~ 0.05 $\mu\text{mol/mol}$ occurred (even when taking into consideration the



206 analytical error bar of ± 0.02 , 2σ), and a slight increase ($0.09 \mu\text{mol/mol}$) is observed between 15 and 13.3 cal kyr
207 BP (B-A period). A rapid increase in the Cd/Ca values beginning at 5.2 cal kyr BP reaches a maximum (0.31
208 $\mu\text{mol/mol}$) during the late Holocene.

209 For core MD77-176, the *H. elegans* Cd/Ca records range between 0.06 and $0.17 \mu\text{mol/mol}$ over the past 18 cal
210 kyr BP (Fig. 2h; supplementary Table S1), without no clear trends and average benthic Cd/Ca values of ~ 0.09
211 $\mu\text{mol/mol}$ during the different periods (HS1, YD and Holocene). However, the benthic Cd/Ca record during the
212 Holocene seems to exhibit a slight increase both in value and range of variations after 6 cal kyr BP.

213

214 **4.2. Foraminifera assemblages of core MD77-191**

215

216 Benthic foraminiferal species richness ranges between 16 and 36, and the total abundance fluctuates between
217 82 and 642 specimens (supplementary Table S2). Hyaline species are the dominant constituents ($>80\%$), and
218 mainly consist of *Bulimina aculeata*, *H. elegans*, *C. pachyderma*, *Uvigerina* spp., *Gyroidina broeckhiana*,
219 *Globocassidulina subglobosa*, *Sphaeroidina bulloides*, *Gyroidinoides* spp., *Lenticulina* spp., *Melonis*
220 *barleeaanum*, and *Globobulimina* spp. (including *Praeglobobulimina* spp.) (in decreasing order of relative
221 average abundance). Agglutinated taxa reach on average about 1.6%, and consist of *Textularia* sp.,
222 *Martinottiella communis*, and *Eggerella bradyi*. The average percentage of porcelaneous species, characterized
223 by *Pyrgo elongata*, *Pyrgo murrhina*, *Pyrgo depressa*, *Pyrgoella irregularis*, *Quinqueloculina* spp., *Sigmoilopsis*
224 *schlumbergeri*, and *Spiroloculina* spp., is about 5.1%.

225 Furthermore, we merged species that share an ecological similarity, such as *Globobulimina affinis*,
226 *Globobulimina pacifica*, and *Praeglobobulimina* spp. into *Globobulimina* spp. A total of 74 samples and 55
227 groups/species were adopted to perform principal component analysis (PCA) in order to identify major faunal
228 trends. The PCA analysis suggests that the benthic foraminifera could be grouped into three assemblages, and
229 represent about 61% of the total variance (Table 1).

230 The combination of *Bulimina aculeata* and *C. pachyderma*, together with *Pullenia bulloides* and
231 *Ehrenbergina trigona* (Figs. 3 and S2), display high positive PC1 loadings. This assemblage, referred hereafter
232 as assemblage 1, dominated the foraminiferal record during the late Holocene (between 6 and 1.4 cal kyr BP).
233 By contrast, *H. elegans* and *Bulimina manginata* exhibit high negative PC1 loadings, and dominate assemblage 2,
234 which corresponds to the record during the early Holocene (Figs. 3 and S2). Other quantitatively important
235 contributors are *C. wuellerstorfi* and *Globocassidulina subglobosa* (Fig. S2).

236 The total variance of PC2 is 19%; for the positive loadings of PC2, *Sphaeroidina bulloides* and *Gyroidinoides*
237 *orbicularis* dominate assemblage 3, which is more important during the last deglaciation (Figs. 3 and S2). The
238 main associated species of assemblage 3 are *Bulimina mexicana* and *Gyroidinoides soldanii* (Fig. S2). However,
239 the main species from negative loadings consist of *Bulimina aculeata*, *H. elegans* and *C. pachyderma*, which
240 dominated the Holocene. The main composition of PC2 negative loadings is dominated by the same benthic
241 species as assemblages 1 and 2, which, as we have seen above, correspond to the Holocene; it is difficult,
242 therefore, to glean any additional information from this regarding bottom conditions. For this reason we only
243 recognize three assemblages in this paper.

244



245 5. Discussion

246 5.1. Past intermediate water Cd_w concentrations from the Northern Indian Ocean

247
248 In the modern ocean, benthic foraminifera Cd/Ca shows a positive correlation with Cd_w and dissolved
249 nutrients (phosphate and nitrate) (Boyle et al., 1976; Hester and Boyle, 1982). As aragonite benthic foraminifera
250 *H. elegans* faithfully records the bottom water Cd concentrations (Cd_w), Cd/Ca ratios can be converted to
251 seawater Cd_w with the appropriate relationship (Eq.1), where the partition coefficient $D_p \approx 1$ for all water depths
252 (Boyle et al., 1995; Bryan and Marchitto, 2010).

253

$$254 D_p = \frac{(Cd/Ca)_{foram}}{(Cd/Ca)_{water}} \quad (Eq.1)$$

255

256 In contrast, the partition coefficient for calcite species changes with water depth. For water depths between
257 1150-3000 m, D_p was calculated based on the equation of Boyle, (1992; Eq. 2). The seawater Ca concentration is
258 assumed to be at a constant, mean value of 0.01 mol/kg (Boyle, 1992).

259

$$260 D_p = 1.3 + (\text{depth} - 1150) \times (1.6/1850) \quad (Eq.2)$$

261

262 The intermediate Cd_w results based on the *H. elegans* Cd/Ca values of core MD77-191, range from 0.5 to 3.1
263 nmol/kg since 17 cal kyr BP (Fig. 4a), with a core top value of 0.80 nmol/kg in agreement with the estimated
264 intermediate water depth modern Cd_w (~0.83 nmol/kg) in the northern Indian Ocean (Boyle et al., 1995).
265 Variations of *H. elegans* Cd_w during the last deglaciation indicate a decrease of about ~0.5 nmol/kg in the HS1
266 and YD periods, with a slight increase (0.9 nmol/kg) during the warm B-A. Cd_w results from core MD77-191
267 indicate a shift from the last deglaciation (~0.8 nmol/kg) to the late Holocene (~1.59 nmol/kg). During the
268 Holocene, the Cd_w records display relatively low values of around 0.9 nmol/kg in the 10-6 cal kyr BP time
269 interval, and show a major shift at around 6.4 cal kyr BP with values rising up to 3.1 nmol/kg.

270 The intermediate Cd_w was also calculated from calcite benthic species *C. pachyderma*, *U. peregrina* and
271 *Globobulimina* spp. from core MD77-191, with values ranging between 0.53-1.48 $\mu\text{mol/mol}$, 0.52-1.04
272 $\mu\text{mol/mol}$ and 0.26-0.65 $\mu\text{mol/mol}$, respectively (Figs. 4b-d). The Cd_w values of *C. pachyderma* and *U.*
273 *peregrina* are within the same range. However, the deep infaunal *Globobulimina* spp. Cd_w displays relatively
274 much lower values and does not exhibit strong variations compared to the other species investigated in this study,
275 displaying a general increasing trend from the last deglaciation to the Holocene. As *Globobulimina* spp.
276 correspond to deep benthic infaunal species, this result may indicate a stable nutrient content of pore water, as
277 compared to other benthic taxa associated with bottom water (Fig. 4d).

278 During the last deglaciation, the Cd_w records of *C. pachyderma* and *U. peregrina* show a decreasing trend
279 during the HS1 and YD events, with mean values of ~ 0.59 and 0.65 nmol/kg for *C. pachyderma* and ~ 0.62 and
280 0.67 nmol/kg for *U. peregrina*, respectively (Fig. 4b and c). The Cd_w records all display higher values during the
281 B-A, with average values of ~ 0.94 and 0.84 nmol/kg, respectively (Fig. 4b and c). The Cd_w records show
282 depleted values in the early Holocene, followed by an abrupt increase during the middle Holocene, with average
283 values of ~0.87 nmol/mol for *C. pachyderma* and ~0.81 nmol/kg for *U. peregrina*.

284 Relative variations in the Cd_w obtained from *C. pachyderma* and *U. peregrina* are in good agreement with the
285 records obtained on *H. elegans*. However, the *H. elegans* Cd_w values are higher than those from the two calcite



286 species, especially during the Late Holocene. Moreover, the core top data of *C. pachyderma* and *U. peregrina*
287 are also lower (~ 0.70 and 0.69 nmol/kg, respectively) than the modern estimated Cd_w data (~ 0.83 nmol/kg) in
288 the northern Indian Ocean (Boyle et al., 1995). These depleted Cd_w values may be related to the benthic
289 foraminiferal microhabitat effect; indeed, *U. peregrina* is known to be strictly a shallow infaunal species, as well
290 as *C. pachyderma* (Fontanier et al., 2002), differing from strictly epifaunal taxa, such as *Cibicides wuellerstorfi*
291 (Mackensen et al., 1993). Thus, when tracking past changes in the bottom water Cd_w concentrations, the use of a
292 strictly epifaunal species living at the water-sediment interface such as *H. elegans* appears to be more robust than
293 using endofaunal species that live in contact with pore water.

294 For core MD77-176, the intermediate water Cd_w calculated from the *H. elegans* Cd/Ca records ranges between
295 0.6 and 1.7 nmol/kg over the past 18 cal kyr BP (Fig. 4e). Compared with intermediate Cd_w from MD77-191, the
296 Cd_w record of core MD77-176 does not display any clear trend from the last deglaciation to the Holocene.
297 However, a slight increase is observed since 6 cal kyr BP, in agreement with the MD77-191 intermediate Cd_w
298 records. In addition, even though the MD77-176 record has a lower time resolution, it displays a shorter
299 maximum (1.3 nmol/kg) during the 13.4-11 cal kyr BP time interval.

300 To summarize, among the three calcite benthic taxa and the aragonitic benthic species *H. elegans*, the Cd/Ca
301 records of *H. elegans* appear to be the most suitable for tracking past Cd_w changes at intermediate water depth
302 through time. Thus, in the following discussion, we will only focus on the intermediate Cd_w calculated from the
303 *H. elegans* Cd/Ca from both studied cores.

304

305 5.2. Comparison between geochemical records and benthic foraminiferal assemblages

306

307 Comparing the geochemical records to the benthic assemblages, we can observe similar patterns. For core
308 MD77-191 from the southeastern Arabian Sea, three benthic assemblages were identified since the last
309 deglaciation. *S. bulloides* and *Gyroidinoides orbicularis* are major components of assemblage 3 (during the last
310 deglaciation), together with *B. mexicana* and *Gyroidinoides soldanii* (Figs. 3 and S2). *S. bulloides* and *B.*
311 *mexicana* are found in intermediate to high organic carbon flux rate regions (e.g., Schmiedl et al., 2000;
312 Eberwein and Mackensen, 2006, 2008), while *G. orbicularis* and *G. soldanii* are associated with well-
313 oxygenated and oligotrophic environments (Peterson, 1984; Burmistrova and Belyaeva, 2006; De and Gupta,
314 2010). Thus, assemblage 3 reflects mesotrophic environments and/or well-ventilated conditions during the last
315 deglaciation. Although millennial-scale changes in the benthic foraminiferal assemblages during the last
316 deglaciation could not be observed, benthic fauna 3 seems at least partly consistent with previous studies in the
317 northern Indian Ocean based on multiple geochemical proxies (e.g., benthic $\delta^{13}C$, intermediate water $[CO_3^{2-}]$ and
318 ϵ_{Nd} records); these studies have revealed the presence of better-ventilated waters, which might correspond to
319 AAIW, during the HS1 and YD (e.g., Yu et al., 2018; Ma et al., 2019; 2020).

320 Benthic foraminiferal assemblage 2 predominates during the early Holocene and is characterized by *H.*
321 *elegans* and *B. manginata* as major contributors (Figs. 3 and S2). The other important contributors are *C.*
322 *wuellerstorfi* and *G. subglobosa*. *B. manginata* is found in high organic carbon flux rate conditions (De Rijk et
323 al., 2000; Eberwein and Mackensen, 2006, 2008). However, previous studies on *H. elegans*, *C. wuellerstorfi* and
324 *G. subglobosa* indicate that these species correspond to high levels of dissolved oxygen and oligotrophic settings
325 (e.g., Altenbach et al., 1999; Fontanier et al., 2002; Murgese and De Deckker, 2005, 2007; De and Gupta, 2010).
326 Periods dominated by these taxa probably indicate high oxygen levels and an oligotrophic environment.



327 Additionally, glacial to Holocene benthic $\delta^{13}\text{C}$ shifts (0.35-0.4‰, vs. PDB) at intermediate-deep water depth in
328 the northern Indian Ocean are interpreted as reflecting an increased contribution of better-ventilated deep water,
329 namely North Atlantic Deep Water (NADW), during the Holocene (e.g., Naqvi et al., 1994; Ma et al., 2019) (Fig.
330 S3). Although the intermediate benthic $\delta^{13}\text{C}$ record from core MD77-191 is missing for the LGM, the average
331 value for the Holocene (\sim 0.31‰, vs. PDB) is consistent with previous studies carried out in the northern Indian
332 Ocean, and may also be associated with well-ventilated conditions (Fig. S3). The predominance of Benthic
333 foraminifera assemblage 2 in the early Holocene seems to be in agreement with the higher values of benthic $\delta^{13}\text{C}$,
334 reflecting better-ventilated water masses, associated with NADW, at the core site.

335 By contrast, *B. aculeata* and *C. pachyderma* are major components of assemblage 1 (during the late Holocene),
336 together with *P. bulloides* and *E. trigona* (Figs. 3 and S2). Living *B. aculeata* have a widespread distribution,
337 with a preference for water depths ranging from 1500 to 2500m, and are typically associated with high organic
338 carbon fluxes (Mackensen et al., 1995; Almogi-Labin et al., 2000; Caille et al., 2015). *P. bulloides* is a shallow
339 infaunal species, which prefers mesotrophic environments and shows adaptability with respect to oxygen
340 concentration in the Arabian Sea (Gupta and Thomas, 1999; Caille et al., 2015). *E. trigona* is commonly
341 recorded in low oxygen habitats (Caille et al., 2015). We thus interpret assemblage 1 as indicating relatively
342 low-oxygen and meso- to eutrophic bottom water conditions during the late Holocene (6-1.4 cal kyr BP).
343 However, the lower oxygen concentrations reflected by benthic fauna 1 seem to be the opposite of what would
344 be expected under an enhanced influence of better ventilated NADW during the Holocene in the northern Indian
345 Ocean. The higher relative abundances of *Globigerina bulloides*, a proxy of upwelling activity, observed in the
346 late Holocene of the same core, MD77-191, suggest increased productivity in the southeastern Arabian Sea
347 (Bassinot et al., 2011) (Fig. 5). This record is synchronous with the benthic foraminiferal assemblage 1 (during
348 the late Holocene). Thus, increased surface productivity during the late Holocene could result in more organic
349 matter in the bottom water, leading to depleted oxygen conditions in bottom water.

350 When we compare benthic assemblages 2 and 3 (during the last deglaciation and early Holocene; 17-6 cal kyr
351 BP) to the fauna 1 (during the late Holocene), assemblages 2 and 3 indicate that intermediate water masses were
352 characterized by higher bottom water oxygen conditions and a lower flux of organic matter. This is associated
353 with depleted *Globigerina bulloides* abundances during the same time interval compared with the late Holocene,
354 suggesting lower productivity in the southeastern Arabian Sea in the period from the last deglaciation to the
355 Holocene (Bassinot et al., 2011) (Fig. 5). Therefore, all of these elements suggest that changes in primary
356 productivity seem to be the main factor impacting on the distribution of benthic assemblages at core MD77-191 site,
357 especially during the Holocene, rather than changes in intermediate-water circulation.

358 In addition, the total organic carbon (C_{org}) could also be used as a qualitative indicator of past productivity
359 and/or bottom water ventilation changes (Naidu et al., 1992; Canfield, 1994; Calvert et al., 1995; Naik et al.,
360 2017). In order to examine the relationships between intermediate C_{d_w} and these different processes (surface
361 productivity and/or water mass ventilation) since the last deglaciation in the eastern Arabian Sea, we compared
362 the MD77-191 C_{d_w} values with the relative abundance of *G. bulloides* and benthic foraminiferal assemblage
363 analyses from the same core MD77-191, together with the records for C_{org} and the *G. bulloides* percentage
364 obtained from core SK237 GC04 (1245m, southeastern Arabian Sea, Naik et al., 2017) (Fig. 5). The MD77-191
365 *H. elegans* C_{d_w} records display a strong co-variation with the C_{org} from core SK237 GC04 since 17 cal kyr BP,
366 and are also in good agreement with the relative abundance of *G. bulloides* records during the Holocene (Fig. 5).



367 In addition, previous studies have suggested that increased Cd_w values (>1 nmol/kg) could correspond to
368 elevated surface productivity (Bostock et al., 2010; Olsen et al., 2016). Thus, we suggest the intermediate Cd_w at
369 core MD77-191 site was mainly influenced by surface productivity, especially during the Holocene.

370 Compared with benthic foraminifera fauna analysis from MD77-191 in the Arabian Sea, the benthic
371 assemblages of core MD77-176 suggest that the intermediate water masses were characterized by oligotrophic to
372 mesotrophic conditions and/or well-ventilated environments during the Holocene (Ma et al., 2019), associated
373 with much lower surface productivity (Fig. S4). This observation is in agreement with low primary productivity
374 during the Holocene reconstructed by the relative abundance of coccolith species *Florisphaera profunda* from
375 the same core MD77-176 in the northeastern BoB (Zhou et al., 2020). In the modern ocean, Prasanna Kumar et
376 al. (2001) indicate that primary productivity in the BoB is much lower than in the Arabian Sea, the lower surface
377 productivity resulting from the large freshwater input from river and direct rainfall as a result of Indian Summer
378 Monsoon precipitation (e.g., Vinayachandran et al., 2002; Madhupratap et al., 2003; Gauns et al., 2005).
379 Moreover, when we compare the average Cd_w value of core MD77-176 from the BoB (~ 0.9 nmol/kg) with
380 results from core MD77-191 in the Arabian Sea (~ 1.2 nmol/kg), lower values, especially during the late
381 Holocene, are in agreement with the benthic assemblages.

382 To sum up, variations in the benthic assemblages seem to be associated with changes in the organic matter
383 flux, linked to surface productivity, especially in the Arabian Sea (Schnitker, 1994). The benthic foraminiferal
384 fauna are consistent with the Cd_w record of core MD77-191 particularly during the late Holocene (6-1.4 cal kyr
385 BP). Thus, our results seem to show that the record of Cd_w is mainly controlled by changes occurring at the
386 surface. However, during the YD, the percentages of planktonic species *G. bulloides* from cores MD77-191 and
387 SK237 GC04 all indicate a slight increase in paleo-productivity, the opposite of what is suggested by the results
388 of core MD77-191 Cd_w and C_{org} obtained from core SK237 GC04. This interval is also marked by enriched *G.*
389 *ruber* $\delta^{18}O$ values, indicating a weaker monsoon and reduced freshwater inputs (Naik et al., 2017). This apparent
390 discrepancy may be related to changes in the intermediate water mass sources and/or ventilation during the last
391 deglaciation. Therefore, we will discuss these issues in greater detail below in order to decipher these different
392 processes.

393

394 5.3. Relationships between primary productivity and monsoon intensity

395

396 During the Holocene, the intermediate Cd_w records obtained from cores MD77-191 and MD77-176 display
397 depleted values in the early Holocene, followed by an abrupt increasing trend at the middle Holocene, and then
398 show a decreasing trend between 5.2 and 2.4 cal kyr BP.

399 Of the two cores, core MD77-176, located in the northeastern BoB, shows the lowest intermediate Cd_w (down
400 to ~ 0.83 nmol/kg) during the 10-6 cal kyr BP time interval. Observations described above suggest that this low
401 in Cd_w resulted from low primary productivity and thus reduced fluxes of organic matter to the intermediate
402 depths. We attribute this evolution to monsoon variation. The early Holocene Climate Optimum (10-6 cal kyr BP)
403 is characterized by enhanced monsoon precipitation (Marzin et al., 2013; Contreras-Rosales et al., 2014) (Figs.
404 6c-e) that resulted in increased freshwater discharge from the Ganges-Brahmaputra river system and from the
405 Irrawaddy River. It is likely that this increase in fresh water drove pronounced ocean stratification in the
406 northeast BoB, inducing low productivity.



407 A similar low in Cd_w is observed in the reconstructed intermediate water Cd_w record from core MD77-191
408 during the early Holocene, with values descending to ~ 0.92 nmol/kg, in the 10-6 cal kyr BP time interval. These
409 low values of intermediate Cd_w are coeval with low surface productivity as recorded by the *G. bulloides*
410 percentage and low values in C_{org} content from SK237 GC04 in the Arabian Sea. Off the southern tip of India,
411 we cannot reject the possibility that increased monsoon precipitation and enhanced freshwater runoffs in the BoB
412 during the early Holocene, inducing a stronger stratification, could explain part of the decrease in surface
413 primary productivity. Yet, at this site, another explanation prevails which is related to the decrease of summer
414 monsoon wind intensity that drives local Eckman pumping. As shown by Bassinot et al. (2011), the productivity
415 variations at the southern tip of India are inversely related to the evolution of upwelling activity along the Oman
416 Margin, to the west of the Arabian Sea. Based on a data/model comparison, Bassinot et al. (2011) showed that
417 this anti-correlation can be attributed to the northward shift of the ITCZ when boreal summer insolation reached
418 a maximum in the early Holocene; this ITCZ location results in enhanced summer monsoon wind intensity and
419 an increase in the associated Eckman pumping in the west of the Arabian Sea, and along the Oman margin, while
420 it weakens at the southern tip of India. This process may thus induce a decrease in surface productivity in the
421 southeastern Arabian Sea.

422 In addition, Naik et al. (2017) pointed out the co-existence of low productivity during the early Holocene in
423 the BoB and to the South of India, in agreement with our data that clearly show the impact of such a reduction of
424 surface primary productivity on the intermediate water Cd_w . These authors suggested a direct relationship
425 between intense monsoon rainfall and reduced surface productivity. However, the northeastern BoB received a
426 much larger amount of river input than the southern tip of India during the early Holocene (Marzin et al., 2013).
427 Thus, it seems reasonable to propose that the northeastern BoB is more affected by the salinity-related
428 stratification effect, while the southern tip of India is more affected by the decrease in wind intensity (Bassinot et
429 al., 2011) with enhanced stratification being potentially made stronger by an additional fresh-water effect,
430 although weaker than in the BoB. Ultimately, both climatic features (summer wind intensity and precipitation)
431 are directly under the control of monsoon evolution resulting from the orbital forcing of low latitude boreal
432 summer insolation.

433 By contrast, higher intermediate Cd_w values from core MD77-191 associated with higher *G. bulloides* relative
434 abundances and C_{org} from core SK237 GC04 during the 5.2-2.4 cal kyr BP time interval could indicate enhanced
435 productivity during the mid to late Holocene (Naik et al., 2017) (Fig. 5). To a lesser extent, this is also observed
436 in the records from the Northern BoB for the same time-period. These changes are consistent with a weakened
437 summer monsoon intensity, with less rainfall during the late Holocene, as observed in the BoB and over the
438 Indian continent (Marzin et al., 2013; Contreras-Rosales et al., 2014; Sarkar et al., 2015), and a progressive
439 increase in monsoon summer winds to the South of India (Bassinot et al., 2011) (Fig. 6). These observations
440 could also strongly support the hypothesis that the major control on surface productivity is linked to monsoon
441 evolution in the BoB and at the southern tip of the Arabian Sea during the Holocene (Bassinot et al., 2011; Naik
442 et al., 2017; Zhou et al., 2020).

443

444 **5.4. Millennial-scale changes in intermediate water circulation during the deglaciation**

445

446 During the last deglaciation, short events have been recorded at the site of core MD77-191 during the 16-15.2



447 (HS1) and 12.6-11 cal kyr BP (YD) time intervals (Fig. 5). The low Cd_w values in the MD77-191 record are
448 coeval with reductions of C_{org} in core SK237 GC04 during the HS1 and YD periods (Fig. 5). According to
449 previous studies, extremely high Cd_w values (>1 nmol/kg) were reported to have been associated with enhanced
450 surface productivity (Bostock et al., 2010; Olsen et al., 2016). However, the range of values of intermediate Cd_w
451 (0.58-0.85 nmol/kg, HS1; 0.5-0.8 nmol/kg, YD) from core MD77-191 during the last deglaciation is much lower
452 compared with the Holocene Cd_w values (>1 nmol/kg), and thus may be associated with other processes such as
453 a better ventilation, changes in the water mass source, and/or depleted surface productivity (Fig. 7). Significant
454 decreases in *G. bulloides* relative abundance of cores SK237 GC04 (Naik et al., 2017) and MD77-191 records
455 were observed from the HS1 to B-A (Bassinot et al., 2011) (Fig. 5). Although a slight increase occurred in the
456 YD, the *G. bulloides* percentage records from both cores show a general depletion during the last deglaciation
457 compared with the last glacial interval and late Holocene (Fig. 5). Thus, we do not expect that surface
458 productivity played an important role during the last deglaciation. In addition, compared with the relative
459 percentage of *G. bulloides* during the B-A, slightly higher values at both core sites during the HS1 and YD may
460 indicate a small, but net increase of surface productivity during these intervals (Fig. 5). This should have led to
461 increased intermediate Cd_w and organic matter preservation under conditions of low oxygen concentration. But,
462 we observe a decrease in these two proxies, the opposite of what would be expected from stronger surface
463 productivity. Thus, this apparent discrepancy provides evidence for the influence of changes in water masses
464 and/or ventilation during the HS1 and YD.

465 Moreover, an increase in benthic $\delta^{13}C$ values is observed during the HS1 and YD in the northern Indian Ocean
466 (e.g., Duplessy et al., 1984; Curry et al., 1988; Naqvi et al., 1994; Jung et al., 2009; Ma et al., 2019). The
467 increase in the different benthic $\delta^{13}C$ records during the HS1 and YD in the western Arabian Sea, Pacific Ocean
468 and BoB is interpreted as reflecting the northward expansion of AAIW (Pahnke and Zahn, 2005; Jung et al.,
469 2009; Ma et al., 2019). The decreased benthic-planktonic foraminiferal ^{14}C offset (B-P age) obtained from
470 marine sediment cores from the Arabian Sea and the Bay of Bengal during the same intervals could confirm
471 enhanced vertical mixing in the Southern Ocean (Bryan et al., 2010; Ma et al., 2019). The transition in the ϵ_{Nd}
472 and $\Delta^{14}C$ records during the deglaciation also indicates a strong northward penetration of AAIW within the
473 North Atlantic and Bay of Bengal (e.g., Cao et al., 2007; Pahnke et al., 2008; Pena et al., 2013; Yu et al., 2018).
474 In addition, during the HS1 and YD, a decrease in the $[CO_3^{2-}]$ record from core MD77-191 also suggests the
475 release of CO_2 from the deep ocean in the deglacial period through the expansion of AAIW (Ma et al., 2020).
476 These time intervals are associated with better ventilation in the Southern Ocean (e.g., Anderson et al., 2009;
477 Skinner et al., 2010), which led to enhanced vertical ventilation resulting in increased production of intermediate
478 water masses (AAIW) (Anderson et al., 2009).

479 As mentioned before, previous studies have suggested an enhanced northward flow of southern sourced
480 intermediate water mass AAIW both in the Atlantic, Pacific and Indian Oceans during the last deglaciation (e.g.,
481 Pahnke et al., 2008; Bryan et al., 2010; Poggemann et al., 2017; Yu et al., 2018; Ma et al., 2019, 2020),
482 indicating that the source of intermediate water masses may be partly the same in these oceans. Thus, by using
483 the benthic $\delta^{13}C$ values collected from the north Indian Ocean to better constrain the influence of AAIW in the
484 two studied cores (Naqvi et al., 1994; Jung et al., 2009; Ma et al., 2019; 2020), we can also compare the range
485 values of AAIW Cd_w obtained from the cores MD77-191 and MD77-176 with other oceans, including data from
486 the Atlantic and Pacific Oceans at intermediate water depth during the HS1 and YD (Cd_w , 0.3-0.9 nmol/kg;



487 Umling et al., 2018; Valley et al., 2017). Unfortunately, the resolution of both intermediate Cd_w and benthic $\delta^{13}C$
488 from core MD77-176 (northeastern BoB) are very low for the HS1 and YD events, making it difficult to extract
489 reliable information. Thus, we have decided to focus on the results from core MD77-191 (0.5-0.85 nmol/kg)
490 during these two time-intervals; these results are in good agreement with the collected dataset (Fig. 7). Thus, the
491 benthic Cd_w results provide new evidence for tracking the northern flow of AAIW in the northern Indian Ocean,
492 which increased during HS1 and the YD.

493 Taken together, Cd_w , B-P age offset, benthic $\delta^{13}C$, ϵ_{Nd} and $\Delta^{14}C$ records reported from the northern Indian
494 Ocean all suggest strong upwelling and enhanced northern flow of AAIW from the Southern Ocean during HS1
495 and the YD. Thus, the variations in these records can provide strong evidence for the hypothesis that Southern
496 Ocean upwelling played a vital role in the increase of atmospheric CO_2 in the deglacial period (Anderson et al.,
497 2009; Skinner et al., 2010, 2014). However, Kohfeld et al. (2005) suggested that although physical processes
498 (such as ventilation) are involved in the glacial-interglacial atmospheric CO_2 change, the biological pump may
499 also contribute nearly half of the observed changes of CO_2 during the glacial-interglacial transitions. As shown
500 above, the HS1 event is characterized by reduced surface productivity, as revealed by the lower percentage
501 values of *G. bulloides* in core MD77-191 (Bassiot et al., 2011) and by several studies of cores located in the
502 eastern and western Arabian Sea within the Oxygen Minimum Zone (e.g., Schulz et al., 1998; Altabet et al.,
503 2002; Ivanochko et al., 2005; Singh et al., 2006, 2011; Naik et al., 2017). This reduced productivity at a
504 millennial timescale suggests that the entire biological factory was related to the reduced monsoon intensity
505 during the North Atlantic Heinrich events (e.g., Singh et al., 2011; Naik et al., 2017). Thus, a weaker biological
506 production could also have contributed to the two-step increase of atmospheric CO_2 during the last deglaciation,
507 at least for the HS1 period.

508

509 6. Conclusions

510

511 Changes in benthic foraminiferal Cd/Ca and assemblages were reconstructed on core MD77-191 (1254 m
512 water depth) located off the southern tip of India, as well as on core MD77-176 (1375 m water depth) from the
513 northern BoB, in order to reveal the evolution of intermediate water circulation and paleo-nutrient changes in the
514 northern Indian Ocean since the last deglaciation. We reconstructed seawater Cd_w concentration by converting *H.*
515 *elegans* Cd/Ca. Benthic Cd/Ca ratios are mainly influenced by changes in surface productivity and intermediate-
516 bottom water ventilation.

517 Results indicate that assemblages 2 and 3, reflecting high bottom water oxygen conditions and a low flux of
518 organic matter, dominated between 17 and 6 cal kyr BP, corresponding to a poor productivity time-period. The
519 typical late Holocene assemblage indicates a relatively low-oxygen level and meso- to eutrophic deep-water
520 conditions, associated with high surface productivity. The early Holocene (10-6 cal ka BP) corresponds to a low
521 in productivity associated with depleted Cd_w in intermediate water. These observations seem to result from
522 enhanced monsoon precipitation and increased river inputs from the Himalayan Rivers, which led to more
523 marked stratification in the BoB and a reduction in primary and export productivity. At the southern tip of India,
524 the decrease in vertical mixing is also associated with a reduction in summer wind forcing resulting from the
525 northward displacement of ITCZ during summer (Bassiot et al., 2011). During the late Holocene (5.2-2.4 cal
526 kyr BP), the increased intermediate Cd_w concentrations of cores MD77-191 and MD77-176 indicate enhanced
527 surface productivity in the southeastern Arabian Sea and in the northeastern BoB, corresponding to weakened



528 monsoon intensity and rainfall, in agreement with other local records and reconstructions of the paleo-monsoon
529 strength. Thus, our results clearly show the strong control of intermediate water Cd_w during the Holocene by
530 orbitally-driven changes in summer monsoon productivity.

531 As far as millennial-scale variability is concerned, during the last deglaciation, decreased intermediate Cd_w
532 concentrations during HS1 and the YD are coeval with increased benthic $\delta^{13}C$, depletion in $[CO_3^{2-}]$ and
533 decreased B-P age offsets. These observations indicate that the low Cd_w values in intermediate water mainly
534 resulted from the increased northward flow of AAIW during HS1 and YD intervals. These signals also provide
535 strong evidence for the important role of enhanced Southern Ocean ventilation in the CO_2 increase during the
536 last deglaciation. The declined intermediate Cd_w obtained from southeastern Arabian Sea (Core MD77-191),
537 combined with the published eastern and western Arabian Sea paleo-productivity results, together provide
538 evidence for the important influence of decreased monsoon intensity at a millennial time scale during cold events
539 in the North Atlantic region, associated with the increase in atmospheric CO_2 during the last deglaciation.

540

541 **Data availability**

542 All data are given in Table 1 and supplementary materials Tables S1-S2.

543

544 **Supplement**

545 The supplement related to this paper is available online.

546

547 **Author contribution**

548 RM, SS, FB and CC developed the idea and interpreted the results. CC and FB supplied foraminifera samples.
549 RM did benthic foraminifera assemblage and geochemical analyses with the aide of FH and LL. ZY and LL
550 joined the discussion. All co-authors helped to improve the article.

551

552 **Competing interests**

553 The authors declare that they have no conflict of interest.

554

555 **Acknowledgements**

556 R. Ma gratefully acknowledges the China Scholarship Council for providing funding for her study in France.
557 The research leading to this paper was funded by the French National Research Agency under the
558 "Investissements d'avenir" programme (Grant ANR-11-IDEX-0004-17-EURE-0006), and the INSU-LEFE-
559 IMAGO-CITRON GLACE project.

560

561 **References**

562

563 Almogi-Labin, A., Schmiedl, G., Hemleben, C., Siman-Tov, R., Segl, M., and Meischner, D.: The influence of
564 the NE winter monsoon on productivity changes in the Gulf of Aden, NW Arabian Sea, during the last 530ka
565 as recorded by foraminifera, *Marine Micropaleontology*, 40 (3), 295–319, 2000.

566 Altabet, M. A., Higginson, M. J., and Murray, R. W.: The effect of millennial-scale changes in the Arabian Sea
567 denitrification on atmospheric CO_2 , *Nature*, 415, 159–162, 2002.



- 568 Altenbach, A. V., Pflaumann, U., Schiebel, R., Thies, A., Timm, S., and Trauth, M.: Scaling percentages and
569 distributional patterns of benthic foraminifera with flux rates of organic carbon, *Journal of Foraminiferal*
570 *Research*, 29 (3), 173–185, 1999.
- 571 Anderson, R. F., Ali, S., Bradtmiller, L. I., Nielsen, S. H. H., Fleisher, M. Q., Anderson, B. E., and Burckle, L.
572 H.: Wind-driven upwelling in the Southern Ocean and the deglacial rise in atmospheric CO₂, *Science*, 323
573 (5920), 1443–1448, 2009.
- 574 Banse, K.: Seasonality of phytoplankton chlorophyll in the central and northern Arabian Sea, *Deep Sea Research*
575 *Part A Oceanographic Research Papers*, 34 (5), 713–723, 1987.
- 576 Barker, S., Greaves, M., and Elderfield, H.: A study of cleaning procedures used for foraminiferal Mg/Ca
577 paleothermometry, *Geochemistry Geophysics Geosystems*, 4 (9), 1–20, 2003.
- 578 Bassinot, F. C., Marzin, C., Braconnot, P., Marti, O., Mathienblard, E., Lombard, F., and Bopp, L.: Holocene
579 evolution of summer winds and marine productivity in the tropical Indian Ocean in response to insolation
580 forcing: Data-model comparison, *Climate of the Past*, 7 (3), 815–829, 2011.
- 581 Bauska, T. K., Baggenstos, D., Brook, E. J., Mix, A. C., Marcott, S. A., Petrenko, V. V., Schaefer, H.,
582 Severinghaus, J. P., and Lee, J. E.: Carbon isotopes characterize rapid changes in atmospheric carbon dioxide
583 during the last deglaciation, *Proceedings of the National Academy of Sciences*, 113(13), 3465–3470, 2016.
- 584 Beal, L. M., Field, A., and Gordon, A. L.: Spreading of Red Sea overflow waters in the Indian Ocean, *Journal of*
585 *Geophysical Research: Oceans*, 105 (C4), 8549–8564, 2000.
- 586 Bostock, H. C., Opdyke, B. N., and Williams, M. J. M.: Characterising the intermediate depth waters of the
587 Pacific Ocean using $\delta^{13}\text{C}$ and other geochemical tracers, *Deep-Sea Research I*, 57 (7), 847–859, 2010.
- 588 Boyle, E. A.: Manganese carbonate overgrowths on foraminifera tests, *Geochim. Cosmochim. Acta*, 63 (18),
589 353–353, 1983.
- 590 Boyle, E. A.: Cadmium: Chemical tracer of deepwater paleoceanography, *Paleoceanography*, 3 (4), 471–489,
591 1988.
- 592 Boyle, E. A.: Cadmium and $\delta^{13}\text{C}$ paleochemical ocean distributions during the stage 2 Glacial Maximum,
593 *Annual Review of Earth and Planetary Sciences*, 20 (1), 245–287, 1992.
- 594 Boyle, E. A. and Keigwin, L. D.: Deep circulation of the north Atlantic over the last 200,000 years: Geochemical
595 evidence, *Science*, 218 (4574), 784–787, 1982.
- 596 Boyle, E. A., Labeyrie, L., and Duplessy, J. C.: Calcitic foraminiferal data confirmed by cadmium in aragonitic
597 *Hoeglundina*: Application to the Last Glacial Maximum in the northern Indian Ocean, *Paleoceanography*, 10
598 (5), 881–900, 1995.
- 599 Boyle, E. A., Sclater, F., and Edmond, J. M.: On the marine geochemistry of Cadmium, *Nature*, 263 (5572), 42–
600 44, 1976.
- 601 Bryan, S. P. and Marchitto, T. M.: Testing the utility of paleonutrient proxies Cd/Ca and Zn/Ca in benthic
602 foraminifera from thermocline waters, *Geochemistry, Geophysics, Geosystems*, 11 (1), 2010.



- 603 Bryan, S. P., Marchitto, T. M., and Lehman, S. J.: The release of ^{14}C -depleted carbon from the deep ocean during
604 the last deglaciation: Evidence from the Arabian Sea, *Earth and Planetary Science Letters*, 298 (1), 244–254,
605 2010.
- 606 Burmistrova, I. I. and Belyaeva, N. V.: Bottom foraminiferal assemblages in the Deryugin Basin (Sea of
607 Okhotsk) during the past 26000 years, *Oceanology*, 46 (6), 834–840, 2006.
- 608 Came, R. E., Oppo, D. W., Curry, W. B., and Lynch-Stieglitz, J.: Deglacial variability in the surface return flow
609 of the Atlantic meridional overturning circulation, *Paleoceanography*, 23, PA1217, 2008.
- 610 Canfield, D. E.: Factors influencing organic carbon preservation in marine sediments, *Chem. Geol.*, 114, 315–329,
611 1994.
- 612 Calvert, S. E., Pedersen, T. F., Naidu, P. D., and von Stackelberg, U.: On the organic carbon maximum on the
613 continental slope of the eastern Arabian Sea, *J. Mar. Res.*, 53, 269–296, 1995.
- 614 Cao, L., Fairbanks, R. G., Mortlock, R. A., and Risk, M. J.: Radiocarbon reservoir age of high latitude north
615 Atlantic surface water during the last deglacial, *Quaternary Science Reviews*, 26 (5), 732–742, 2007.
- 616 Caille, C., Mojtahid, M., Gooday, A. J., Jorissen, F. J., and Kitazato, H.: Living (rose-bengal-stained) benthic
617 foraminiferal faunas along a strong bottom-water oxygen gradient on the Indian margin (Arabian Sea),
618 *Biogeosciences*, 12 (16), 5005–5019, 2015.
- 619 Contreras-Rosales, L. A., Jennerjahn, T., Tharammal, T., Meyer, V., Lückge, A., Paul, A., and Schefuß, E.:
620 Evolution of the Indian Summer Monsoon and terrestrial vegetation in the Bengal region during the past 18
621 ka, *Quaternary Science Reviews*, 102, 133–148, 2014.
- 622 Corliss, B. H.: Recent deep-sea benthonic foraminiferal distributions in the southeast Indian Ocean: Inferred
623 bottom-water routes and ecological implications, *Marine Geology*, 31 (1-2), 115–138, 1979.
- 624 Corliss, B. H., Martinson, D. G., and Keffer, T.: Late Quaternary deep-ocean circulation, *Geological Society of
625 America Bulletin*, 97 (9), 1106, 1986.
- 626 Curry, W. B., Duplessy, J. C., Labeyrie, L. D., and Shackleton, N. J.: Changes in the distribution of $\delta^{13}\text{C}$ of deep
627 water σ_{CO_2} between the last glaciation and the Holocene, *Paleoceanography*, 3 (3), 317–341, 1988.
- 628 Curry, W. B., Ostermann, D. R., Guptha, M. V. S., and Ittekkot, V.: Foraminiferal production and monsoonal
629 upwelling in the Arabian Sea: evidence from sediment traps, *Geological Society, London, Special
630 Publications*, 64, 93–106, 1992.
- 631 De, S. and Gupta, A. K.: Deep-sea faunal provinces and their inferred environments in the Indian Ocean based
632 on distribution of recent benthic foraminifera, *Palaeogeography, Palaeoclimatology, Palaeoecology*, 291 (3),
633 429–442, 2010.



- 634 De Rijk, S., Jorissen, F. J., Rohling, E. J., and Troelstra, S. R.: Organic flux control on bathymetric zonation of
635 Mediterranean benthic foraminifera, *Marine Micropaleontology*, 40, 151–166, 2000.
- 636 Den Dulk, M., Reichart, G. J., Memon, G. M., Roelofs, E. M. P., Zachariasse, W. J., and Zwaan, G. J. V. D.:
637 Benthic foraminiferal response to variations in surface water productivity and oxygenation in the northern
638 Arabian Sea, *Marine Micropaleontology*, 35 (1–2), 43–66, 1998.
- 639 Duplessy, J. C., Shackleton, N. J., Matthews, R. K., Prell, W., Ruddiman, W. F., Caralp, M., and Hendy, C. H.:
640 ^{13}C record of benthic foraminifera in the last interglacial ocean: Implications for the carbon cycle and the
641 global deep water circulation, *Quaternary Research*, 21 (2), 225–243, 1984.
- 642 Eberwein, A. and Mackensen, A.: Live and dead benthic foraminifera and test $\delta^{13}\text{C}$ record primary productivity
643 off Morocco (NW-Africa), *Deep-Sea Research. Part I*, 53 (8), 1379–1405, 2006.
- 644 Eberwein, A. and Mackensen, A.: Last Glacial Maximum paleoproductivity and water masses off NW-Africa:
645 Evidence from benthic foraminifera and stable isotopes, *Marine Micropaleontology*, 67, 87–103, 2008.
- 646 Elderfield, H. and Rickaby, R. E. M.: Oceanic Cd/P ratio and nutrient utilization in the glacial Southern Ocean,
647 *Nature*, 405 (6784), 305–310, 2000.
- 648 Fontanier, C., Jorissen, F. J., Licari, L., Alexandre, A., Anschutz, P., and Carbonel, P.: Live benthic
649 foraminiferal faunas from the Bay of Biscay: Faunal density, composition, and microhabitats, *Deep Sea
650 Research Part I: Oceanographic Research Papers*, 49 (4), 751–785, 2002.
- 651 Gauns, M., Madhupratap, M., Ramaiah, N., Jyothibabu, R., Fernandes, V., Paul, J. T., and Prasanna Kumar, S.:
652 Comparative accounts of biological productivity characteristics and estimates of carbon fluxes in the Arabian
653 Sea and the Bay of Bengal, *Deep-Sea Research II*, 52, 2003–2017, 2005.
- 654 Gomes, H., Goes, J., and Saino, T.: Influence of physical processes and freshwater discharge on the seasonality
655 of phytoplankton regime in the Bay of Bengal, *Continental Shelf Research*, 20, 313–330, 2000.
- 656 Gupta, A. K. and Thomas, E.: Latest Miocene-Pleistocene productivity and deep-sea ventilation in the
657 Northwestern Indian Ocean (Deep Sea Drilling Project Site 219), *Paleoceanography*, 14(1), 62–73, 1999.
- 658 Gupta, A. K., Anderson, D. M., and Overpeck, J. T.: Abrupt changes in the Asian Southwest Monsoon during
659 the Holocene and their links to the North Atlantic Ocean, *Nature*, 421 (6921), 354–357, 2003.
- 660 Hammer, Ø., Harper, D. A. T., and Ryan, P. D.: Past: Paleontological statistics software package for education
661 and data analysis, 2001.
- 662 Hall, J. M. and Chan, L. H.: Ba/Ca in benthic foraminifera: Thermocline and middepth circulation in the north
663 Atlantic during the last glaciation, *Paleoceanography*, 19, PA4018, 2004.



- 664 Hermelin, J. O. R.: Relative abundances of benthic foraminifera in ODP hole 117-728A, PANGAEA, 1991.
- 665 Hermelin, J. O. R.: Variations in the benthic foraminiferal fauna of the Arabian Sea: A response to changes in
666 upwelling intensity? Geological Society, London, Special Publications, 64, 151–166, 1992.
- 667 Hermelin, J. O. R. and Shimmield, G. B.: Impact of productivity events on the benthic foraminiferal fauna in the
668 Arabian Sea over the last 150,000 years, *Paleoceanography*, 10 (1), 85–116, 1995.
- 669 Hertzberg, J. E., Lund, D. C., Schmittner, A., and Skrivaneck, A. L.: Evidence for a biological pump driver of
670 atmospheric CO₂ rise during Heinrich Stadial 1, *Geophysical Research Letters*, 43(23), 12,242–12,251, 2016.
- 671 Hester, K. and Boyle, E.: Water chemistry control of Cadmium content in recent benthic foraminifera, *Nature*,
672 298, 260–262, 1982.
- 673 Holbourn, A., Henderson, A. S., and Macleod, N.: Front matter. In *Atlas of benthic foraminifera*, pp. 1–641,
674 2013.
- 675 Ivanochko, T. S., Ganeshram, R. S., Brummer, G. J. A., Ganssen, G., Jung, S. J. A., Moreton, S. G., and Kroon,
676 D.: Variations in tropical convection as an amplifier of global climate change at the millennial scale, *Earth
677 Planet. Sci. Lett.*, 235, 302–314, 2005.
- 678 Jaccard, S. L., Galbraith, E. D., Martínez-García, A., and Anderson, R. F.: Covariation of deep Southern Ocean
679 oxygenation and atmospheric CO₂ through the last ice age, *Nature*, 530(7589), 207–210, 2016.
- 680 Jones, R. W.: *The challenger foraminifera*, Oxford University Press, 1994.
- 681 Jung, S. J. A., Kroon, D., Ganssen, G., Peeters, F., and Ganeshram, R.: Enhanced Arabian Sea intermediate
682 water flow during glacial North Atlantic cold phases, *Earth and Planetary Science Letters*, 280 (1), 220–228,
683 2009.
- 684 Kohfeld, K. E., Quéré, C. L., Harrison, S. P., and Anderson, R. F.: Role of marine biology in Glacial-interglacial
685 CO₂ cycles, *Science*, 308, 74, 2005.
- 686 Lévý, M., Shankar, D., André, J.-M., Shenoi, S., Durand, F., and De Boyer Montégut, C.: Basin-wide seasonal
687 evolution of the Indian Ocean's phytoplankton blooms, *Journal of Geophysical Research*, 112 (C12014), 1–
688 14, 2007.
- 689 Loeblich, A. R. and Tappan, H.: Generic taxa erroneously regarded as foraminifers. In *Foraminiferal genera and
690 their classification*, Loeblich, A. R., Tappan, H., Eds. Springer US: Boston, MA, pp. 726–730, 1988.
- 691 Lynch-Stieglitz, J., Fairbanks, R. G., and Charles, C. D.: Glacial-interglacial history of Antarctic Intermediate
692 Water: Relative strengths of Antarctic versus Indian Ocean sources, *Paleoceanography*, 9 (1), 7–29, 1994.



- 693 Ma, R., Sépulcre, S., Bassinot, F., Haurine, F., Tisn érat-Laborde, N., and Colin, C.: North Indian Ocean
694 circulation since the last deglaciation as inferred from new elemental ratio records for benthic foraminifera
695 *Hoeglundina elegans*, *Paleoceanography and Paleoclimatology*, 35, 2020.
- 696 Ma, R., Sépulcre, S., Licari, L., Bassinot, F., Liu, Z., Tisn érat-Laborde, N., Kallel, N., Yu, Z., and Colin, C.:
697 Changes in intermediate circulation in the Bay of Bengal since the Last Glacial Maximum as inferred from
698 benthic foraminifera assemblages and geochemical proxies, *Geochemistry, Geophysics, Geosystems*, 20,
699 1592–1608, 2019.
- 700 Mackensen, A., Hubberten, H. W., Bickert, T., Fischer, G., and Fütterer, D. K.: $\delta^{13}\text{C}$ in benthic foraminiferal
701 tests of *Fontbotia wuellerstorfi* (Schwager) relative to $\delta^{13}\text{C}$ of dissolved inorganic carbon in Southern Ocean
702 deep water: implications for Glacial ocean circulation models, *Paleoceanography*, 6, 587–610, 1993.
- 703 Mackensen, A., Schmiedl, G., Harloff, J., and Giese, M.: Deep-sea foraminifera in the South Atlantic Ocean;
704 ecology and assemblage generation, *Micropaleontology*, 41 (4), 342–358, 1995.
- 705 Madhupratap, M., Gauns, M., Ramaiah, N., Prasanna Kumar, S., Muraleedharan, P. M., Sousa, S. N., and
706 Muraleedharan, U.: Biogeochemistry of the Bay of Bengal: physical, chemical and primary productivity
707 characteristics of the central and western Bay of Bengal during summer monsoon 2001, *Deep-Sea Research*
708 II, 50, 881–896, 2003.
- 709 Marchitto, T. M. and Broecker, W. S.: Deep water mass geometry in the glacial atlantic ocean: A review of
710 constraints from the paleonutrient proxy Cd/Ca, *Geochemistry, Geophysics, Geosystems*, 7, 2006.
- 711 Marchitto, T. M., Lehman, S. J., Ortiz, J. D., Flückiger, J., and Geen, A. V.: Marine radiocarbon evidence for the
712 mechanism of deglacial atmospheric CO_2 rise, *Science*, 316, 1456–1459, 2007.
- 713 Marra, J. and Barber, R. T.: Primary productivity in the Arabian Sea: A synthesis of JGOFS data, *Progress in*
714 *Oceanography*, 65 (2), 159–175, 2005.
- 715 Marzin, C., Kallel, N., Kageyama, M., Duplessy, J. C., and Braconnot, P.: Glacial fluctuations of the Indian
716 monsoon and their relationship with north Atlantic climate: New data and modelling experiments, *Clim. Past*,
717 9 (5), 2135–2151, 2013.
- 718 McCorkle, D. C., Martin, P. A., W. Lea, D. W., and Klinkhammer, G. P.: Evidence of a dissolution effect on
719 benthic foraminiferal shell chemistry: $\delta^{13}\text{C}$, Cd/Ca, Ba/Ca, and Sr/Ca results from the ontong Java Plateau,
720 *Paleoceanography*, 10 (4), 699–714, 1995.
- 721 Mi éneck, V. M.: S édimentation et dissolution des carbonates biog éniques aux moyennes latitudes Nord et Sud,
722 Approche quantitative et relations avec les pal éocirculations oc éaniques des derniers 150 000 ans. PhD thesis,
723 Universit éBordeaux I, pp. 277, 1997.
- 724 Monnin, E., Inderm ühle, A., D älenbach, A., Fl ückiger, J., Stauffer, B., Stocker, T. F., Raynaud, D., and Barnola,



- 725 J. M.: Atmospheric CO₂ concentrations over the last glacial termination, *Science*, 291 (5501), 112–114, 2001.
- 726 Murgese, D. S. and De Deckker, P.: The distribution of deep-sea benthic foraminifera in core tops from the
727 eastern Indian Ocean, *Marine Micropaleontology*, 56 (1), 25–49, 2005.
- 728 Murgese, D. S. and De Deckker, P.: The late quaternary evolution of water masses in the eastern Indian Ocean
729 between Australia and Indonesia, based on benthic foraminifera faunal and carbon isotopes analyses,
730 *Palaeogeography, Palaeoclimatology, Palaeoecology*, 247 (3), 382–401, 2007.
- 731 Naqvi, W. A., Charles, C. D., and Fairbanks, R. G.: Carbon and oxygen isotopic records of benthic foraminifera
732 from the northeast Indian Ocean: Implications on glacial-interglacial atmospheric CO₂ changes, *Earth and
733 Planetary Science Letters*, 121 (1), 99–110, 1994.
- 734 Naidu, P. D., Prakash Babu, C., and Rao, C. M.: The upwelling record in the sediments of the western
735 continental margin of India, *Deep-Sea Res.*, 39, 715–723, 1992.
- 736 Naidu, P. D. and Malmgren, B. A.: A high-resolution record of late Quaternary upwelling along the Oman
737 margin, Arabian Sea based on planktonic foraminifera, *Paleoceanography*, 11, 129–140, 1996.
- 738 Naik, D. K., Saraswat, R., Lea, D. W., Kurtarkar, S. R., and Mackensen, A.: Last glacial-interglacial productivity
739 and associated changes in the eastern Arabian Sea, *Palaeogeography, Palaeoclimatology, Palaeoecology*, 483,
740 147–156, 2017.
- 741 O'Malley, R.: Ocean productivity. <http://www.science.oregonstate.edu/ocean.Productivity/index.php>. 2017.
- 742 Olsen, A., Key, R. M., van Heuven, S., Lauvset, S. K., Velo, A., Lin, X., and Suzuki, T.: The Global Ocean Data
743 Analysis Project version 2 (GLODAPv2) – an internally consistent data product for the world ocean, *Earth
744 System Science Data*, 8(2), 297–323, 2016.
- 745 Olson, D. B., Hitchcock, G. L., Fine, R. A., and Warren, B. A.: Maintenance of the low-oxygen layer in the
746 central Arabian Sea, *Deep-Sea Research Part II: Tropical Studies In Oceanography*, 40(3), 673–685. 1993.
- 747 Oppo, D. W. and Fairbanks, R. G.: Variability in the deep and intermediate water circulation of the Atlantic
748 Ocean during the past 25,000 years: Northern Hemisphere modulation of the Southern Ocean, *Earth and
749 Planetary Science Letters*, 86, 1–15, 1987.
- 750 Pahnke, K., Goldstein, S. L., and Hemming, S. R.: Abrupt changes in Antarctic Intermediate Water circulation
751 over the past 25,000 years, *Nature Geoscience*, 1, 870, 2008.
- 752 Pahnke, K. and Zahn, R.: Southern Hemisphere water mass conversion linked with north Atlantic climate
753 variability, *Science*, 307 (5716), 1741–1746, 2005.
- 754 Pena, L. D., Goldstein, S. L., Hemming, S. R., Jones, K. M., Calvo, E., Pelejero, C., and Cacho, I.: Rapid
755 changes in meridional advection of Southern Ocean intermediate waters to the tropical Pacific during the last



- 756 30kyr, *Earth and Planetary Science Letters*, 368, 20–32, 2013.
- 757 Peterson, L. C.: Recent abyssal benthic foraminiferal biofacies of the eastern Equatorial Indian Ocean, *Marine*
758 *Micropaleontology*, 8 (6), 479–519, 1984.
- 759 Phillips, S. C., Johnson, J. E., Giosan, L., and Rose, K.: Monsoon-influenced variation in productivity and
760 lithogenic sediment flux since 110 ka in the offshore Mahanadi Basin, northern Bay of Bengal, *Marine and*
761 *Petroleum Geology*, 58, 502–525, 2014.
- 762 Pichevin, L. E., Reynolds, B. C., Ganeshram, R. S., Cacho, I., Pena, L., Keefe, K., and Ellam, R. M.: Enhanced
763 carbon pump inferred from relaxation of nutrient limitation in the glacial ocean, *Nature*, 459(7250), 1114–
764 1117, 2009.
- 765 Poggemann, D. W., Hathorne, E., Nuernberg, D., Frank, M., Bruhn, I., Reißig, S., and Bahr, A.: Rapid deglacial
766 injection of nutrients into the tropical Atlantic via Antarctic Intermediate Water, *Earth and Planetary Science*
767 *Letters*, 463, 118–126, 2017.
- 768 Prasanna Kumar, S., Madhupratap, M., Dileep Kumar, M., Muraleedharan, P. M., de Souza, S. N., Gauns, M.,
769 and Sarma, V. V. S. S.: High biological productivity in the central Arabian Sea during the summer monsoon
770 driven by Ekman pumping and lateral advection, *Current Science*, 81, 1633–1638, 2001.
- 771 Prell, W. L. and Kutzbach, J. L.: Monsoon variability over the past 150,000 years, *Journal of Geophysical*
772 *Research Atmospheres*, 92 (D7), 8411–8425, 1987.
- 773 Reid, J. L.: On the total geostrophic circulation of the south Pacific Ocean: Flow patterns, tracers and transports,
774 *Progress in Oceanography*, 16 (1), 1–61, 2003.
- 775 Rostek, F., Bard, E., Beaufort, L., Sonzogni, C., and Ganssen, G. M.: Sea surface temperature and productivity
776 records for the past 240 kyr in the Arabian Sea, *Deep Sea Research Part II: Topical Studies in Oceanography*,
777 44(6-7), 1461–1480, 1997.
- 778 Saraswat, R., Nigam, R., and Correge, T.: A glimpse of the Quaternary monsoon history from India and
779 adjoining seas, *Palaeogeography, Palaeoclimatology, Palaeoecology*, 397, 1–6, 2014.
- 780 Sarkar, S., Prasad, S., Wilkes, H., Riedel, N., Stebich, M., Basavaiah, N., and Sachse, D.: Monsoon source shifts
781 during the drying mid-Holocene: Biomarker isotope based evidence from the core ‘monsoon zone’ (CMZ) of
782 India, *Quaternary Science Reviews*, 123, 144–157, 2015.
- 783 Schlitzer, R.: Ocean data view. <http://odv.awi.de>, 2015.



- 784 Schmiiedl, G., De Bovee, F., Buscail, R., Charriere, B., Hemleben, C., Medernach, L., and Picon, P.: Trophic
785 control of benthic foraminiferal abundance and microhabitat in the bathyal Gulf of Lions, western
786 Mediterranean Sea, *Marine Micropaleontology*, 40, 167–188, 2000.
- 787 Schmiiedl, G., Hemleben, C., Keller, J., and Segl, M.: Impact of climatic changes on the benthic foraminiferal
788 fauna in the Ionian Sea during the last 330,000 years, *Paleoceanography*, 13 (5), 447–458, 1998.
- 789 Schnitker, D.: Deep-sea benthic foraminifers: Food and bottom water masses. In: Zahn, R., Pedersent, T. F.,
790 Kaminski, M. A., Labeyrie, L. (eds), *Carbon cycling in the glacial ocean: Constraints on the ocean's role in
791 global change. NATO ASI Series (Series I: Global Environmental Change)*, vol 17, Springer, Berlin,
792 Heidelberg, 1994.
- 793 Schott, F. A. and McCreary, J. P.: The monsoon circulation of the Indian Ocean, *Progress in Oceanography*, 51,
794 1–123, 2001.
- 795 Schulz, H., von Rad, U., and Erlenkeuser, H.: Correlation between Arabian Sea and Greenland climate
796 oscillation of the past 110,000 years, *Nature*, 393, 54–57, 1998.
- 797 Shankar, D., Vinayachandran, P. N., and Unnikrishnan, A. S.: The monsoon currents in the north Indian Ocean,
798 *Progress in Oceanography*, 52(1):63–120, 2002.
- 799 Singh, A. D., Jung, S. J. A., Darling, K., Ganeshram, R., Ivanochko, T., and Kroon, D.: Productivity collapses in
800 the Arabian Sea during glacial cold phases, *Paleoceanography*, 26, PA3210, 2011.
- 801 Singh, A. D., Kroon, D., and Ganeshram, R.: Millennial scale variations in productivity and OMZ intensity in
802 the eastern Arabian Sea, *Journal of the Geological Society of India*, 68 (3), 369–377, 2006.
- 803 Skinner, L. C., Claire, W., Scrivner, A. E., and Fallon, S. J.: Radiocarbon evidence for alternating northern and
804 southern sources of ventilation of the deep Atlantic carbon pool during the last deglaciation, *PNAS*, 111 (15),
805 5480–5484, 2014.
- 806 Skinner, L. C., Fallon, S., Waelbroeck, C., Michel, E., and Barker, S.: Ventilation of the deep Southern Ocean
807 and deglacial CO₂ rise, *Science*, 328 (5982), 1147–1151, 2010.
- 808 Stuiver, M. and Grootes, P. M.: GISP2 oxygen isotope ratios, *Quaternary Research*, 53, 277–284, 2000.
- 809 Tachikawa, K. and Elderfield, H.: Microhabitat effects on Cd/Ca and δ¹³C of benthic foraminifera, *Earth and
810 Planetary Science Letters*, 202, 607–624, 2002.
- 811 Talley, L. D., Pickard, G. L., Emery, W. J., and Swift, J. H.: Preface. In *Descriptive physical oceanography
812 (sixth edition)*, Academic Press: Boston, pp. 1–383, 2011.



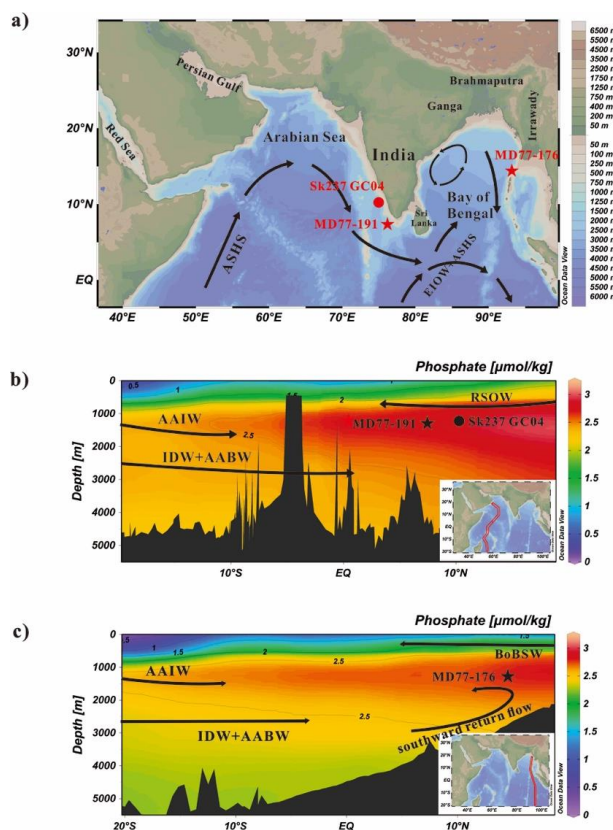
- 813 Thushara, V. and Vinayachandran, P. N.: Formation of summer phytoplankton bloom in the northwestern Bay of
814 Bengal in a coupled physical-ecosystem model, *Journal of Geophysical Research: Oceans*, 121 (12), 8535–
815 8550, 2016.
- 816 Toggweiler, J. R.: Variation of atmospheric CO₂ by ventilation of the ocean’s deepest water, *Paleoceanography*,
817 14, 571–588, 1999.
- 818 Umling, N. E., Thunell, R. C., and Bizimis, M.: Deepwater expansion and enhanced remineralization in the
819 eastern equatorial Pacific during the Last Glacial Maximum, *Paleoceanography and Paleoclimatology*, 33,
820 563–578, 2018.
- 821 Valley, S., Lynch-Stieglitz, J., and Marchitto, T. M.: Timing of deglacial AMOC variability from a high-
822 resolution seawater Cadmium reconstruction: Timing deglacial upper amoc variability, *Paleoceanography*, 32,
823 1195–1203, 2017.
- 824 Vinayachandran, P. N., Murty, V. S. N., and Ramesh Bahu, V.: Observations of barrier layer formation in the
825 Bay of Bengal during summer monsoon, *Journal of Geophysical Research*, 107, 8018, 2002.
- 826 Van der Zwaan, G. J., Duijnste, I. A. P., Den Dulk, M., Ernst, S. R., Jannink, N. T., and Kouwenhoven, T. J.:
827 Benthic foraminifers: Proxies or problems? A review of paleocological concepts, *Earth-Science Reviews*, 46
828 (1), 213–236, 1999.
- 829 Xie, R. C., Marcantonio, F., and Schmidt, M. W.: Deglacial variability of Antarctic Intermediate Water
830 penetration into the north Atlantic from authigenic Neodymium isotope ratios, *Paleoceanography*, 27,
831 PA3221, 2012.
- 832 Yu, Z., Colin, C., Ma, R., Meynadier, L., Wan, S., Wu, Q., Kallel, N., Sepulcre, S., Dapoigny, A., and Bassinot,
833 F.: Antarctic Intermediate Water penetration into the northern Indian Ocean during the last deglaciation,
834 *Earth and Planetary Science Letters*, 500, 67–75, 2018.
- 835 Yu, J., Menviel, L., Jin, Z. D., Thornalley, D. J. R., Foster, G. L., Rohling, E. J., McCave, I. N., McManus, J. F.,
836 Dai, Y., Ren, H., He, F., Zhang, F., Chen, P. J., and Roberts, A. P.: More efficient North Atlantic carbon
837 pump during the Last Glacial Maximum, *Nat. Commun.*, 10, 2019.
- 838 Zhou, X., Duchamp-Alphonse, S., Kageyama, M., Bassinot, F., Beaufort, L., and Colin, C.: Dynamics of
839 primary productivity in the northeastern Bay of Bengal over the last 26 000 years, *Clim. Past Discuss.*, in
840 review, 2020.
- 841 Ziegler, M., Diz, P., Hall, I. R., and Zahn, R.: Millennial-scale changes in atmospheric CO₂ levels linked to the
842 Southern Ocean carbon isotope gradient and dust flux, *Nature Geoscience*, 6, 457–461, 2013.
- 843
844
845



846 **Table 1.** Species composition of benthic foraminiferal assemblages from core MD77-191.

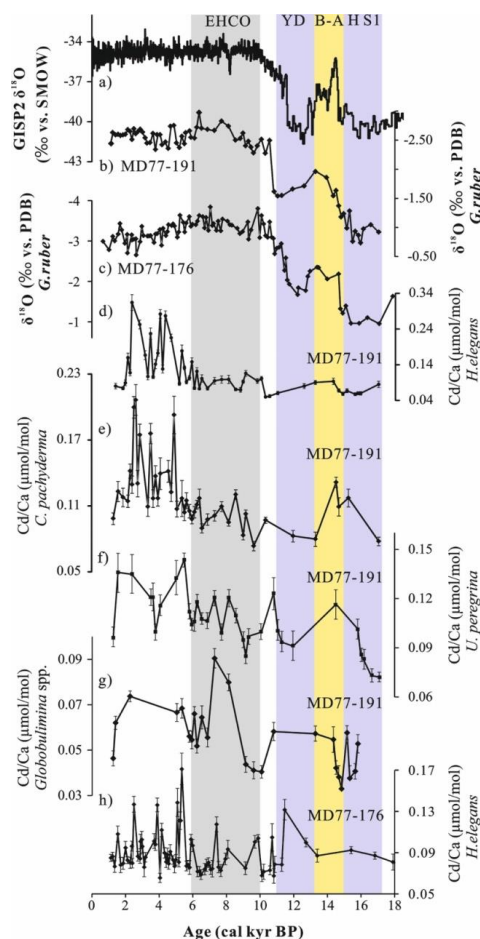
	Dominant species		Important associated species	Variance (%)
PC1				42
Positive loadings	<i>Bulimina aculeata</i>	0.84	<i>Pullenia bulloides</i>	0.18
	<i>Cibicidoides pachyderma</i>	0.19	<i>Ehrenbergina trigona</i>	0.13
Negative loadings	<i>Hoeglundina elegans</i>	-0.14	<i>Cibicidoides wuellerstorfi</i>	-0.04
	<i>Bulimina manginata</i>	-0.07	<i>Globocassidulina subglobosa</i>	-0.06
PC2				19
Positive loadings	<i>Sphaeroidina bulloides</i>	0.42	<i>Gyroidinoides orbicularis</i>	0.17
	<i>Bulimina mexicana</i>	0.11	<i>Gyroidinoides soldanii</i>	0.07
Negative loadings	<i>Bulimina aculeata</i>	-0.14	<i>Hoeglundina elegans</i>	-0.62
	<i>Cibicidoides pachyderma</i>	-0.07		

847
848



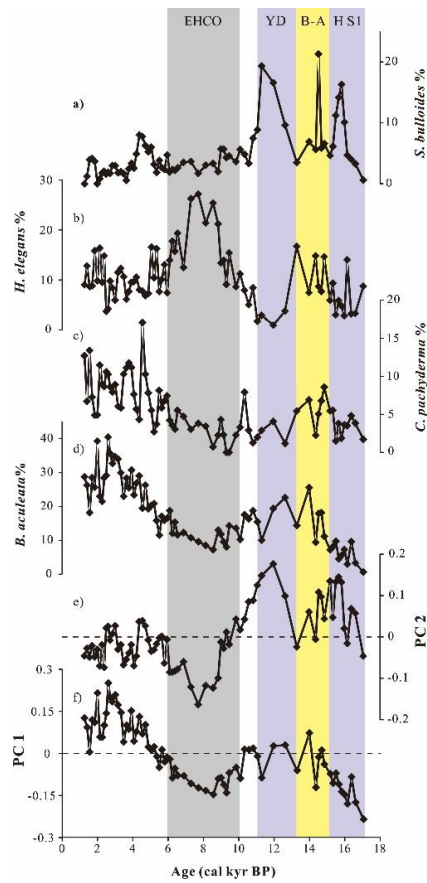
849
 850
 851
 852
 853
 854
 855
 856
 857
 858
 859
 860
 861

Fig. 1. (a) Oceanographic setting and locations of core MD77-191 in the Arabian Sea (red star), core MD77-176 in the Bay of Bengal (red star) and reference site SK237 GC04 (red circle, Naik et al., 2017). The black arrows represent the general surface circulation direction in the Northern Indian Ocean during the summer, Southwest Monsoon (Schott and McCreary, 2001). (b) and (c) Phosphate distribution along depth-latitude sections during the Southwest Monsoon and Northeast Monsoon periods, for the Arabian Sea and the Bay of Bengal, respectively. Data (in $\mu\text{mol/kg}$, colored scale) were contoured and plotted using the Ocean Data View (ODV) software (Schlitzer, 2015). On these two figures are shown the distribution and circulation of water masses in the Arabian Sea and Bay of Bengal (black arrows). ASHS: Arabian Sea High Salinity Water, EIOW: Eastern Indian Ocean Water, BoBSW: Bay of Bengal surface waters, AAIW: Antarctic Intermediate Water, RSOW: Red Sea Overflow Water, AABW: Antarctic Bottom Water, IDW: Indian Deep Water.



862
863

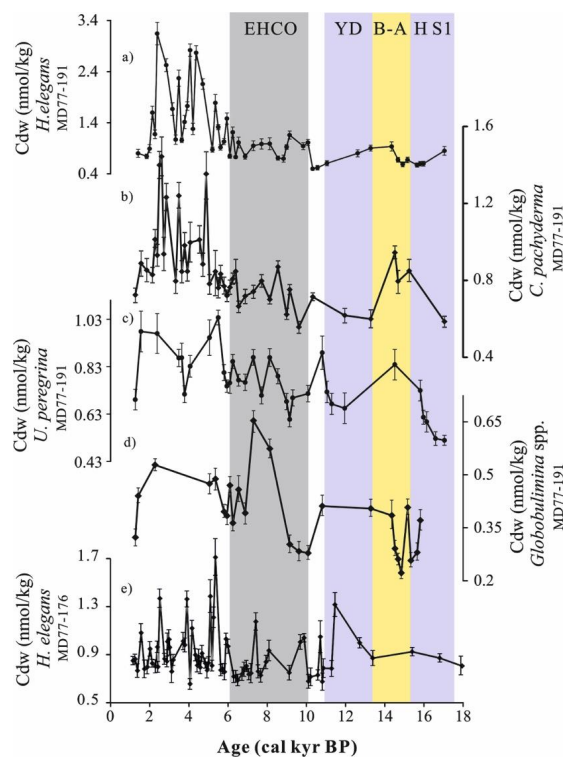
864 **Fig. 2.** (a) GISP2 Greenland ice core $\delta^{18}\text{O}$ signal (Stuiver and Grootes, 2000). (b)-(c) *Globigerinoides ruber* $\delta^{18}\text{O}$
865 records of cores MD77-191 and MD77-176, respectively (Marzin et al., 2013; Ma et al., 2020). (d)-(g) Cd/Ca
866 records of the benthic foraminifera *Hoeglundina elegans*, *Cibicidoides pachyderma*, *Uvigerina peregrina*, and
867 *Globobulimina* spp. obtained from core MD77-191; (h) Cd/Ca records of the benthic foraminifera *H. elegans*
868 from core MD77-176. EHCO for Early Holocene Climate Optimum, YD for Younger Dryas, B-A for Bølling-
869 Allerød and HS1 for Heinrich stadial 1.



870

871

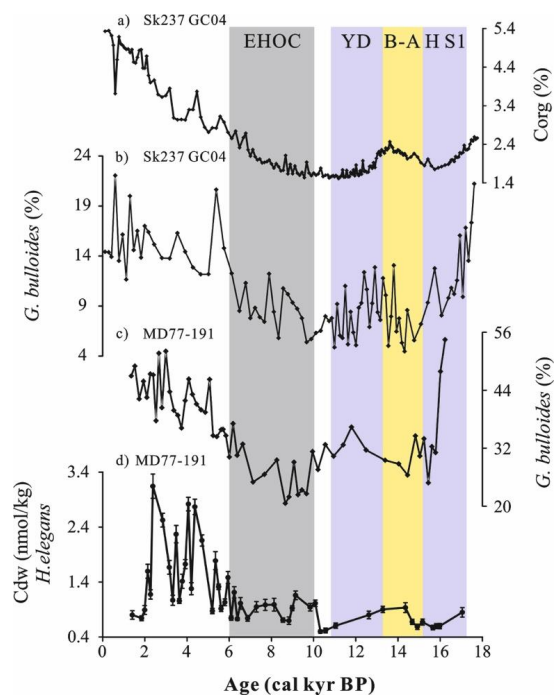
872 **Fig. 3.** Down core variations of PC scores and the percentages of major species. The color shaded intervals and
873 abbreviations are the same as in Figure 2.



874

875

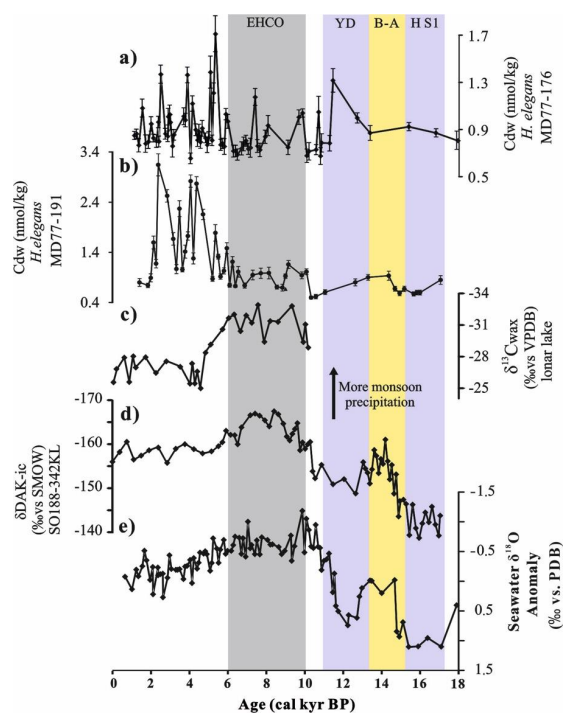
876 **Fig. 4.** (a)-(d) Cd_w records calculated based on the Cd/Ca of benthic foraminifera *Hoeglundina elegans*,
877 *Cibicides pachyderma*, *Uvigerina peregrina*, and *Globobulimina* spp. obtained from core MD77-191, (e) Cd_w
878 record from core MD77-176 reconstructed using *H. elegans* Cd/Ca. The color shaded intervals and abbreviations
879 are the same as in Figure 2.



880

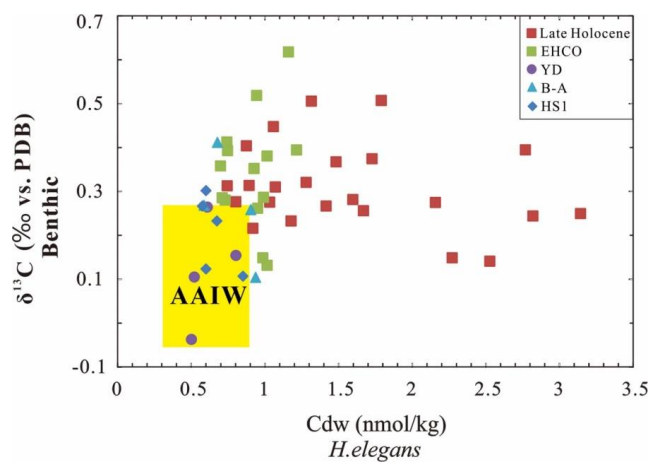
881

882 **Fig. 5.** (a) Organic carbon weight percentage (%C_{org}) and (b) *G. bulloides* percentage from core SK237 GC04
883 (1245m, Arabian Sea, Naik et al., 2017). (c) Relative abundance of *G. bulloides* (Ml áneck, 1997; Bassinot et al.,
884 2011) and (d) Cd_w records from core MD77-191 (Arabian Sea). The color shaded intervals and abbreviations are
885 the same as in Figure 2.



886
887
888
889
890
891
892
893
894
895
896

Fig. 6. (a) and (b) intermediate Cd_w calculated from *H. elegans* obtained from MD77-176 and MD77-191, respectively. (c) Lonar Lake $\delta^{13}C_{wax}$ record (Sarkar et al., 2015). (d) δDAK_{ic} record from core SO188-342KL (Contreras-Rosales et al., 2014). (e) Seawater $\delta^{18}O$ anomaly obtained from MD77-176 (Marzin et al., 2013). The color shaded intervals and abbreviations are the same as in Figure 2.



897
898

899 **Fig. 7.** Intermediate Cd_w versus benthic $\delta^{13}C$ obtained from core MD77-191 located off the southern tip of India.
900 The yellow shaded area represents the ranges of Cd_w - $\delta^{13}C$ values of AAIW during the HS1 and YD, which were
901 reconstructed in the Indian Ocean (benthic $\delta^{13}C$, Naqvi et al., 1994; Jung et al., 2009; Ma et al, 2019; 2020),
902 Pacific and Atlantic Oceans (benthic Cd_w , Valley et al., 2017; Umling et al., 2018) at intermediate water depths.
903 The abbreviations are the same as in Figure 2.